Signature of f-electron conductance in α-Ce single-atom contacts

Sebastian Kuntz,[1] Oliver Berg,[1] Christoph Sürgers,[1,*] and Hilbert v. Löhneysen[1,2]

[1]*Physikalisches Institut, Karlsruhe Institute of Technology, P.O. Box 6980, 76049 Karlsruhe, Germany*

[2]*Institut für Festkörperphysik, Karlsruhe Institute of Technology, P.O. Box 3640, 76021 Karlsruhe, Germany*

(Received 23 November 2016; revised manuscript received 31 July 2017; published 14 August 2017)

Cerium is a fascinating element exhibiting, with its different phases, long-range magnetic order and superconductivity in bulk form. The coupling of the $4f$ electron to sd conduction electrons and to the lattice is responsible for unique structural and electronic properties like the isostructural first-order solid-solid transition from the cubic γ phase to the cubic α phase, which is accompanied by a huge volume collapse of 14%. We report experiments aiming at disentangling the $4f$ contribution to the electric conductance of the different phases. On single-atom Ce contacts we observe a strongly enhanced conductance G. By controlling the content of α-Ce employing different rates of cooling, we find a strong correlation between the fraction of α-Ce and the magnitude of G at the last conductance plateau before the contact breaks. We attribute the enhanced conductance of α-Ce to the additional contribution of the $4f$ level.

DOI: 10.1103/PhysRevB.96.085120

I. INTRODUCTION

Cerium is perhaps the elemental material that exhibits the most pronounced configurational changes. Under ambient pressure, Ce is in the fcc phase (γ-Ce) in the configuration $[\mathrm{Xe}](6s5d)^3 4f^1$, with the $4f$ electron strongly localized, and exhibits Curie-Weiss-type paramagnetism [1,2]. However, below $\sim$200 K in the ground state of α-Ce the $4f$ electron is delocalized [3]. α-Ce has the same fcc structure as γ-Ce, but the lattice constant a changes from 5.15 to 4.85 Å. It is noteworthy that α'-Ce, a high-pressure variant of the α phase, is even superconducting with $T_c = 1.7$ K [4,5]. Cerium is thus a paradigm of the interplay of magnetism and superconductivity.

The early proposal describing the $\gamma \rightarrow \alpha$ phase transition by the promotion of the f electron to the sd conduction band [1,6] was found to be in disagreement with subsequent experiments [7–10] and, furthermore, not confirmed by band-structure calculations [11]. Instead, a delocalization of the $4f$ electron into a $4f$ band in α-Ce was suggested, pointing towards an orbitally selective Mott transition (MT) [7,12].

The nature of the γ-α transition, which can be tuned at ambient temperature by hydrostatic pressure, is still under debate [13–15]. The issue is complicated by the existence of an intervening ($320 \geqslant T \geqslant 170$ K) double-hcp phase (β-Ce). The β phase has electronic properties similar to those of the γ phase, with localized $4f$ moments that order antiferromagnetically below 12.5 K [16,17]. This has been confirmed by density functional theory (DFT) in the local-density approximation taking the on-site Hubbard interaction into account (LDA + U) [18]. The γ-α transition proceeds much faster than the γ-β transition. Since the transitions between these phases are of first order, it is very difficult to obtain single-phase Ce modifications [16,19].

Although the structural and electronic properties of α-, β-, and γ-Ce have been studied experimentally and theoretically for decades, the different contributions of s, d, and f electrons to the total conductance have not been resolved. Mechanically controlled break junctions (MCBJs) offer the possibility to approach the quantum regime where the magnitude of the conductance is of the order of a few conductance quanta, $G_0 = 2e^2/h$ [20]. Here the conductance G exhibits plateaulike features when the contact is gradually opened mechanically, intercepted by sharp steps to lower G. It has been demonstrated for many different metals that the transport at the last plateau before breakage is due to current flow through a single atom [20]. The conductance on the last plateau, on the order of G_0, depends on the number of atomic valence orbitals at or close to the Fermi level E_F and on the transmission coefficients of the orbitals [21]. Therefore, this technique is well suited to investigate atomic-size contacts of elemental metals with different electron configurations like cerium. We note in passing that the situation in metals differs distinctly from that in semiconductors. In the latter, conductance quantization, i.e., $G = nG_0$, with n being integer, has been observed because the inverse Fermi wave number k_F^{-1} is much larger than the interatomic distance a due to the small conduction-electron density. In metals, on the other hand, $k_\mathrm{F}^{-1} \approx a$, leading to a strong intertwining of electronic properties and atomic structure in the contact. Here we report on the conductance of Ce single-atom contacts of MCBJs on the last plateau at 4.2 K, i.e., single-atom contacts, obtained from polycrystalline wires which underwent different thermal treatments to obtain samples with different fractions of α-Ce.

II. EXPERIMENT

A. Sample preparation

All samples were prepared from the same Ce starting material (purity 99.99%, Atlantic Equipment Engineers). This was first melted several times in an arc furnace under argon atmosphere to obtain a homogeneous ingot. After heating, the melt solidified rapidly by cooling to 18 °C in approximately 1 min by contact with a water-cooled copper plate. The material prepared in this manner was labeled q-Ce. The ingot was cut into two halves, one of which was thermally annealed. For this purpose, it was put in an alumina crucible and sealed in a quartz tube under argon atmosphere ($p \approx 5\times10^{-2}$ mbar). The quartz tube was thermally annealed for several days.

*christoph.suergers@kit.edu

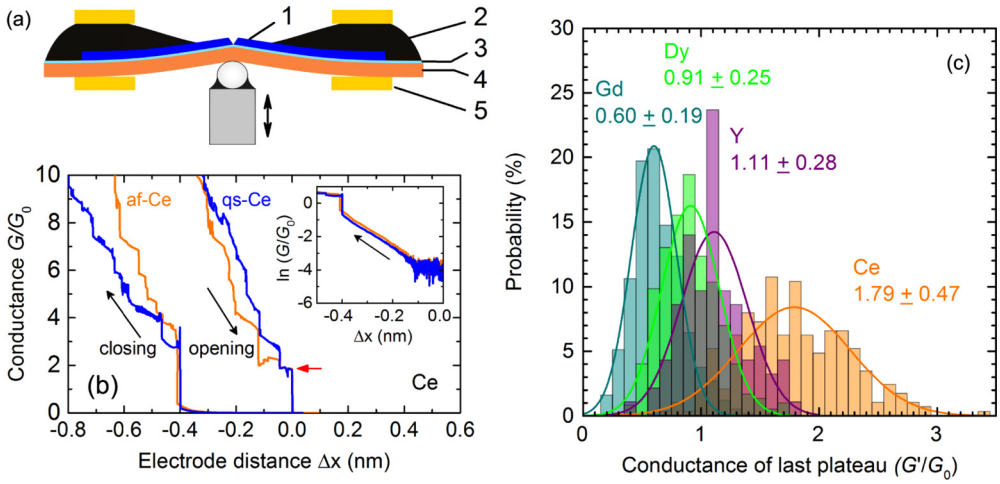

FIG. 1. (a) Schematic of a mechanically controlled break junction. 1: Notched Ce wire, 2: Stycast epoxy, 3: insulating Durimide layer, 4: bendable phosphor-bronze substrate, and 5: countersuppports. (b) Conductance G vs electrode distance (proportional to piezo voltage) of a cerium break junction at 4.2 K. The red arrow marks the conductance of the last plateau before breaking. The inset shows semilogarithmic plots of the conductance vs electrode distance while closing the contact. The linear behavior $\ln(G/G_0) \propto \Delta x$ observed below the jump to contact at $\Delta x \approx -0.4$ nm is characteristic for electron tunneling. (c) Histograms of the conductance G' of the last plateau of Gd, Dy [22], Y, and Ce nanocontacts with a bin size of $0.1G'/G_0$. For each histogram, the total probability integrated over all events is 100%. Solid lines represent a Gaussian distribution fit to the data with the mean value $\bar{G}'$ and standard deviation σ indicated.

First, the temperature was raised to $T = 600\,^{\circ}$C to cross the γ-β phase boundary and then held there for 8 h. Afterwards, the temperature was lowered over a period of about 4 d to $T = 100\,^{\circ}$C and then lowered even more slowly, with a cooling rate of $\partial T/\partial t = 3\,^{\circ}$C/h, while crossing the γ-β phase boundary ($T_{\gamma,\beta} \approx 60\,^{\circ}$C). The material prepared in this manner was labeled a-Ce.

B. Measuring methods

X-ray diffraction was done using a Siemens D500 powder diffractometer equipped with a ^{4}He flow cryostat and with the sample under high vacuum ($p = 10^{-7}$ mbar). Pieces of 0.5-mm thickness were cut from the ingot in several arbitrary spatial directions. They were properly cleaned in acetone, and their oxide layers were carefully removed with a scalpel and then polished with abrasive sandpaper. Afterwards, they were immediately covered with a thin film of highly diluted GE varnish to protect them against further oxidation. X-ray diffractograms were obtained in θ-2θ Bragg-Brentano mode using Cu K_α radiation and a Ni foil to reduce the contribution from Cu K_β radiation.

Resistivity data were taken on bulk Ce samples that were subjected to the different heat treatments described above in a physical property measurement system (PPMS, Quantum Design) in a four-point probe setup. Cerium pieces of $0.5\times0.5\times10$ mm size were cut off the ingots and contacted with copper wires using a conductive epoxy (EPO-TEK H20E).

For the MCBJs, thin wires of 0.1×0.1 mm^2 cross section and 8-mm length were cut from the ingot. A notch was cut in the middle of the wire as a predetermined point where it should break during bending. The wire was glued with Stycast epoxy to a flexible 0.3-mm-thick copper-bronze substrate coated with a 2-μm-thick Durimide film for electrical insulation. It was crucial to heavily coat the sample with Stycast for stabilization of the wire sustaining the structural $\gamma \rightarrow \alpha$ phase transition (with intervening β phase), which is accompanied by a huge volume change and thus generation of mechanical stress. The Ce wire was connected with conductive epoxy (EPO-TEK H20E) to four copper leads in order to perform four-point conductance measurements. This assembly was then mounted in the MCBJ device shown in Fig. 1(a) with countersupports 8 mm apart and cooled to 4.2 K in a ^{4}He bath cryostat. The substrate was bent mechanically by pushing a piston against the back of the substrate, and fine tuning of the bending was achieved by using a piezo stack controlled by a voltage V_p. A voltage of 10 μV was applied to the junction, and the current through the junction was measured. The electrode distance Δx was obtained from $G(V_p)$ in the tunneling regime by using appropriate work functions of the materials as described earlier [22]. All conductance measurements on the MCBJ devices were carried out at 4.2 K.

III. RESULTS

Figure 1(b) shows the conductance G in units of G_0 vs the electrode distance Δx of cerium contacts at 4.2 K. Here Δx was determined from conductance measurements in the tunneling regime, and the distance zero was arbitrarily set to the onset of conductance upon closing the contact signaled by a discontinuous jump from $G \ll G_0$ to $G \approx G_0$. The curves are typical of conductance curves of many elemental metals [20]. Upon stretching the contact, the conductance decreases by showing several steps due to the structural relaxation of the material and reformation of the atomic structure at the neck until, finally, a last plateau [Fig. 1(b), red arrow] is reached before the contact eventually breaks and the conductance jumps to zero. Usually, this behavior is evaluated statistically on a large number of curves to reveal the most frequently occurring conductance values [20].

Here we focus on the conductance G' of the last plateau before breaking at 4.2 K, characteristic of the conductance of a single-atom contact, for some rare-earth-metal contacts in Fig. 1(c). While for ferromagnetic Gd, ferromagnetic dysprosium [22], and nonmagnetic yttrium we observe a distribution (described by a Gaussian distribution; see below) of G' with a maximum at $\bar{G}' = 0.6G_0$, $\bar{G}' = 0.91G_0$, and $\bar{G}' = 1.11G_0$, respectively, a broader distribution with a maximum at $\bar{G}' = 1.79G_0$ is observed for this particular contact of cerium. The values of $\bar{G}'$ for Dy and Y are close to G_0, as likewise observed for $3d$ transition metals [20]. The conductance for Gd is in agreement with a recent investigation of lithographically prepared Gd MCBJs, where the conductance histogram, taking into account all plateaus observed below $20G_0$, revealed a maximum at $0.75G_0$ [23]. The electronic transport through atomic contacts is usually considered ballistic, where the conductance is expressed by transport channels with a certain transmission of the electronic wave function in the Landauer-Büttiker theory [20]. The strongly enhanced conductance of Ce single-atom contacts compared to transition metals and to the rare-earth metals Gd and Dy with localized $4f$ conduction electrons suggests that additional transport channels contribute to the total conductance of Ce which are attributed to the $4f$ orbital. We further note that the standard deviations σ (indicating the width of the distribution) in Fig. 1(c) for Gd, Dy, and Y are of the order of $0.2G_0$–$0.3G_0$, which is typical for polyvalent metals, in particular for Fe, Ni, and Co with partially filled $3d$ shells [24]. Due to the localized nature of the $4f$ electrons in Gd and Dy, which are not expected to contribute to conduction, the width arises from sd hybridization, which strongly depends on the structure of the particular contact under consideration. The observed large width $\sigma \approx 0.5$ of Ce contacts strongly suggests that the local environment of the Ce atom in the contact strongly affects the f-$(sd)^3$ hybridization.

Detailed DFT calculations of bulk Ce incorporating electronic correlations via the Gutzwiller approximation [15] indeed showed that at the critical volume of the γ-α transition, the absolute value of the f-sd hopping energy is much larger and changes much more strongly than the f-f hopping energy. Thus, the large width of σ for Ce contacts comes as no surprise and, in fact, underscores the contribution of the $4f$ electrons to the conductance.

In order to investigate the effect of the $4f$ configuration on single-atom Ce contacts, we employed the content of α-Ce in our Ce samples as a control parameter. To this end, we subjected the Ce ingots to different heat treatments. The q-Ce samples were quenched from the melt to room temperature. These samples passed very quickly through the γ-β transition and are expected to contain a large volume fraction of α-Ce at low T. The a-Ce samples were annealed at 600 °C and slowly cooled to 100 °C. The γ-β transition ($T_{\gamma\beta} = 60$°C) was passed even more slowly to 40 °C at a rate of 3 °C/h. These samples are expected to contain a larger volume fraction of β-Ce and a smaller fraction of α-Ce at low temperatures. The samples were then cooled from room temperature to low temperatures, and their structure was checked by x-ray diffraction with Cu K_α radiation, as shown in Fig. 2.

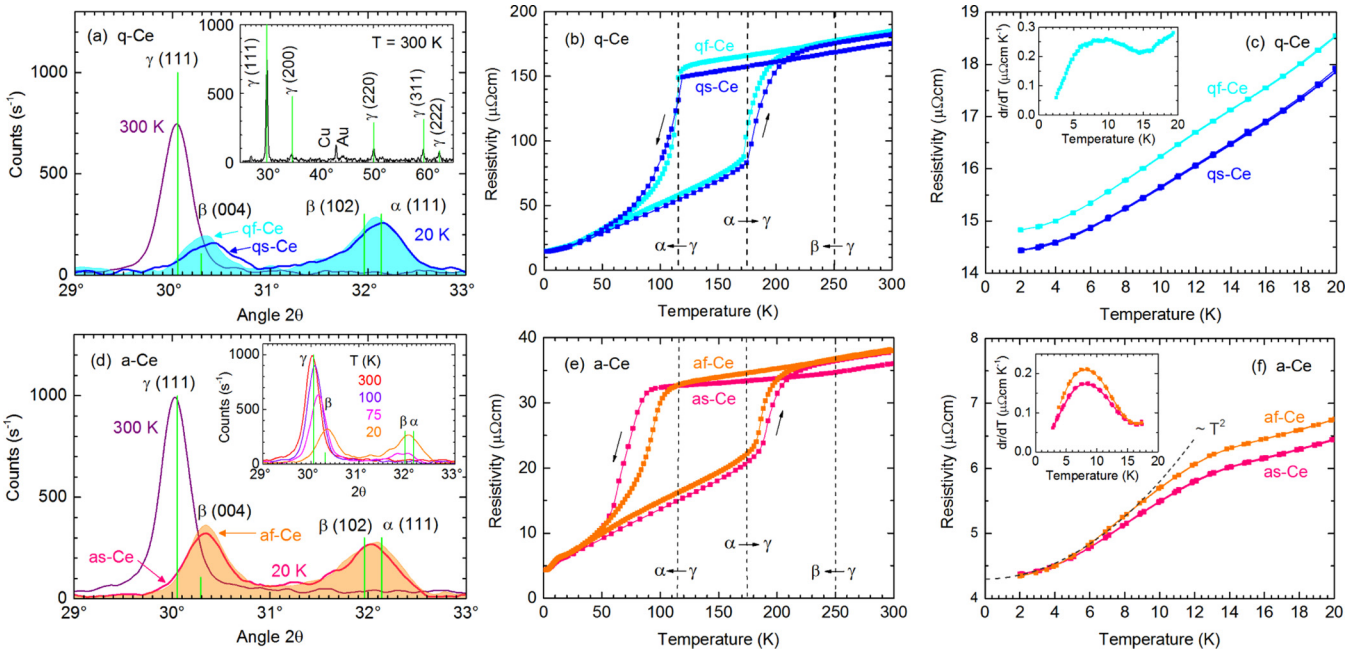

FIG. 2. (a) X-ray diffractogram of q-Ce at 300 and 20 K. Colored area indicates the intensity obtained after fast cooling from 300 to 20 K (qf-Ce); solid lines indicate intensities measured after slow cooling (qs-Ce). Green bars mark reflections according to the International Centre for Diffraction Data (ICDD) database for α-Ce (No. 78-0640), β-Ce (No. 89-2728), and γ-Ce (No. 78-0638). The inset shows the full diffractogram at 300 K, where "Cu" and "Au" indicate contributions arising from the sample holder. (b) Resistivity cycles vs temperature of q-Ce for fast and slow cooling and heating. Dashed vertical lines indicate the transition temperature for the $\gamma \rightarrow \beta$, $\gamma \rightarrow \alpha$, and $\alpha \rightarrow \gamma$ phase transitions according to Ref. [25]. (c) Resistivity of the second cooling cycle. The inset shows the derivative $d\rho/dT$ vs temperature. (d)–(f) X-ray diffraction and resistivity data of sample a-Ce similar to (a)–(c). The inset in (d) shows the reflections for different temperatures. The dashed line in (f) indicates a $\rho \propto T^2$ behavior. The inset shows $d\rho/dT$ vs T.

TABLE I. Ratio S_α of integrated x-ray intensities and resistivity ratio $RR_\beta = \rho(15K)/\rho(2K)$ for the different Ce samples cooled with different rates from 300 to 20 K. $\bar{G}'_i$, $\bar{\sigma}_i$, and A_i are the mean values, standard deviations, and areas of the Gaussian distribution functions, respectively, shown in Fig. 3. χ_1^2 and χ_2^2 are the χ^2 values using one and two distribution functions, respectively.

Sample	Cooling (K min^{-1})	S_α	RR_β	$\bar{G}' \pm \sigma$ (units of G_0)	A	χ_1^2	$\bar{G}'_1 \pm \sigma_1$ (units of G_0)	A_1	$\bar{G}'_2 \pm \sigma_2$ (units of G_0)	A_2	χ_2^2
as-Ce	1	0.49	1.62	1.54 ± 0.45	52.9	6.34	1.53 ± 0.52	42.1	1.57 ± 0.29	11.8	5.60
af-Ce	10	0.51	1.59	1.71 ± 0.37	72.0	12.96	1.61 ± 0.29	53.6	2.10 ± 0.26	17.4	10.89
qs-Ce	1	0.65	1.47	1.77 ± 0.40	28.2	8.78	1.48 ± 0.20	10.8	1.98 ± 0.25	15.7	7.89
qf-Ce	10	0.67	1.39	1.74 ± 0.47	29.2	10.08	1.51 ± 0.30	16.1	2.12 ± 0.35	12.5	8.73

At room temperature $T = 300$ K all Bragg reflections can be assigned to the γ phase of cerium [see inset in Fig. 2(a)]. The intensities of the individual Bragg reflections deviate from the intensities expected for a powder of randomly distributed grains due to a preferred orientation of some crystallites along the [111] direction in the polycrystalline ingot. Upon cooling to 20 K, the $\gamma(111)$ reflection shifts to larger angles (smaller lattice-plane distances) and is at 20 K attributed to the $\beta(004)$ reflection. Below 100 K an additional peak develops around $2\theta = 32^\circ$ [see inset in Fig. 2(d)] due to the transformation to the α phase below 100 K. Figures 2(a) and 2(d) clearly show that a phase mixture of α-Ce and γ-Ce forms at low temperatures with a higher fraction of α-Ce in q-Ce compared to a-Ce. Furthermore, the fraction depends on whether the sample was cooled quickly (qf-Ce, af-Ce; colored areas) or slowly (qs-Ce, as-Ce; solid lines). For a quantitative estimate of the fraction of α-Ce at 20 K, we estimate the ratio S_α of the integrated intensities I at $2\theta = 30.3^\circ$ and 32.1°, $S_\alpha = I(32.1^\circ)/[I(32.1^\circ) + I(30.3^\circ)]$. Table I shows that the fast-cooled qf-Ce has a much larger S_α and hence fraction of α-Ce than the slowly cooled as-Ce. These results are in perfect agreement with earlier investigations by Gschneidner *et al.* [25].

The phase transformations are also observed in the temperature dependence of the resistivity [see Figs. 2(b) and 2(e)], for which the annealed a-Ce exhibits a factor of 5 lower resistivity than q-Ce which was rapidly cooled from the melt. In both samples, the resistivity drops while cooling through the $\gamma \rightarrow \alpha$ transition and strongly increases while heating through the $\alpha \rightarrow \gamma$ transition, with a hysteresis characteristic of a first-order phase transition. For q-Ce, the temperatures where the resistive transitions set in agree again very well with data by Gschneidner *et al.* [25]. In contrast, the hysteresis observed for a-Ce is much broader, possibly due to the larger amount of β phase hampering and delaying the transformation from γ- to α-Ce [26].

At temperatures below 20 K, a-Ce shows a kink in $\rho(T)$ around 12 K [Fig. 2(f)] characteristic of the onset of antiferromagnetic order in β-Ce [16,26]. In the antiferromagnetic regime, the resistivity follows a $\rho \propto T^2$ dependence due to antiferromagnetic spin waves [27]. The kink is only weakly observed in q-Ce [Fig. 2(c)]. We use the resistivity ratio $RR_\beta = \rho(15\,\mathrm{K})/\rho(2\,\mathrm{K})$ to indicate the amount of β phase in the sample. Table I shows that the relative amount of β phase decreases from slowly cooled as-Ce to quickly cooled qf-Ce, in agreement with the corresponding increase in the fraction of α-Ce estimated from the x-ray intensity ratio S_α. In summary, samples with different volume fractions of α-Ce and β-Ce at low temperatures have been successfully prepared and characterized by x-ray diffraction and resistivity data.

IV. DISCUSSION

We now turn to the conductance properties of the different Ce nanocontacts. We proceed by considering the conductance value of the last plateau G' [Fig. 1(b)] and plot in Fig. 3 histograms of four representative samples thus focusing on single-atom-contact histograms instead of those of full conductance curves $G(\Delta x)$. These histograms comprise only opening curves because closing curves generally show much larger last-plateau values extending up to $5G_0$. This suggests that upon closing the contacts, instantaneously, several atoms form the contact.

We first note that the conductance values G' of the samples can be described by a Gaussian distribution (gray curves),

$$N(G') = \frac{A}{\sigma\sqrt{2\pi}} \exp\left[\frac{-(G' - \bar{G}')^2}{2\sigma^2}\right], \qquad (1)$$

where A is the area, $\bar{G}'$ is the mean value, and σ is the standard deviation. However, the G' values of the a-Ce samples follow $N(G')$ much more closely and smoothly than the q-Ce samples. This is also quantitatively seen from χ_1^2 in Table I. The different values of $\bar{G}'$ indicate that it is the thermal treatment of the wires which has an effect on the conductance. The most striking difference is seen by comparing the distributions of as-Ce and qf-Ce [see inset in Fig. 3(d)]. As mentioned above, the a-Ce samples contain more β phase with localized stable Ce^{3+} moments. It is highly plausible that the local environment of atoms in the contact with a reduced number of nearest neighbors leads to a further stabilization of localized moments. This observation suggests that it is not the hybridization of $4f$ electrons with intra-atomic $6s/5d$ orbitals but, rather, the hybridization with nearest-neighbor orbitals which is essential. The hybridization possibly further decreases while opening the contact due to the elongation of interatomic bonds when a single atom forms the contact. Indeed, scanning tunneling spectroscopy on single Ce or Co impurities on the Ag or Cu surface shows a strong reduction of the Kondo temperature T_K for thin layers and for single atoms and clusters compared to T_K of the corresponding bulk solids due to the reduction in the number of nearest neighbors and the ensuing decrease in hybridization of the magnetic impurity with respect to the bulk electronic system of the host crystal [28–30]. In contrast, for individual Co adatoms on Cu(100), T_K strongly increases toward the bulk value upon decreasing the tip-adatom distance due to the stronger hybridization between the Co $3d$ level

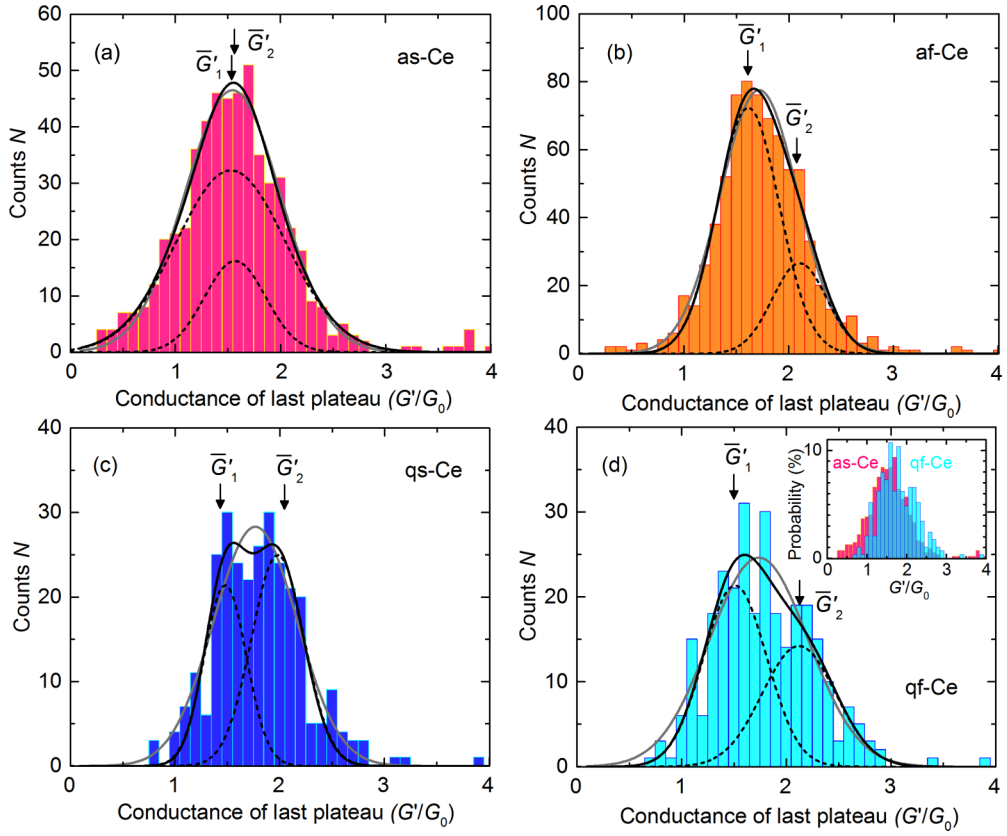

FIG. 3. Histograms of the conductance G' of the last plateau of differently prepared Ce MCBJs, with a bin size of $0.1G'/G_0$. The gray solid lines indicate a fit of a single Gauss curve to the distribution. The black solid line shows the sum of two Gauss curves indicated by dashed lines. Parameters of the fits are given in Table 1. The inset in (d) shows the rescaled distributions of as-Ce and qf-Ce for comparison.

and the conduction-electron states of the Cu substrate and the W tip [31]. In line with these arguments a substantial change in the $4f$ electronic structure at the surface of α-Ce towards a γ-like behavior was observed in photoemission experiments [32]. Therefore, in the as-Ce samples with a large fraction of β-Ce and stabilization of Ce^{3+} moments in the contact region, a homogeneous distribution of G' is expected.

The χ^2 of the fitted distribution curves can be further reduced by considering two Gaussians centered at mean values $\bar{G}'_1$ and $\bar{G}'_2$ (see the solid and dashed black curves in Fig. 3). The corresponding parameters shown in Table I were iteratively obtained by varying four parameters while keeping two parameters constant until χ^2_2 did not decrease further. In contrast to the as-Ce samples, for which we obtain two similar values of $\bar{G}'_1 = 1.53$ and $\bar{G}'_2 = 1.57$, in agreement with the value $\bar{G}' = 1.54$ when using only one Gaussian (Table I), the af-Ce sample is actually better described by a dominant Gaussian centered at $\bar{G}'_1 = 1.6G_0$ and a smaller Gaussian centered at $\bar{G}'_2 = 2.1G_0$, indicating that fast cooling from room temperature also favors the α-phase formation to some extent. On the other hand, the histograms of the q-Ce samples can be decomposed into two Gaussians, one centered around $\bar{G}'_1 \approx 1.5G_0$ and the other around $\bar{G}'_2 \approx 2G_0$. These two components correspond to stable Ce moments reminiscent of the β phase (G'_1) and strongly hybridized moments as in the α phase (G'_2) with a finite transmission probability due to their more delocalized nature, respectively. Table I summarizes this behavior; that is, samples with a larger volume fraction of α-Ce, represented by a large S_α and a small RR_β, more frequently show a higher conductance G'_2 of the last plateau inferred from the ratio of the areas A_1 and A_2 of the two distribution functions. The enhanced conductance clearly depends on the sample treatment and the different volume fraction of electronically different phases.

Unfortunately, it was not possible to obtain reliable I-V curves of the contacts that would demonstrate the appearance or absence of a zero-bias conductance peak or Fano resonance. Such measurements are hampered by the low mechanical stability and high sensitivity to mechanical vibrations of MCBJs made from bulk wires compared to MCBJs made from films microstructured by e-beam lithography.

We now discuss the implication of our results for the γ-α transition. In both Kondo volume collapse (KVC) and MT models the f electrons are strongly correlated in the α and γ phases, and both models are in qualitative agreement with the localization-delocalization picture. Specifically, the MT model of f electrons considers localized nonbonding f states in γ-Ce which are favored by the on-site f-f Coulomb interaction U mentioned above being larger than the f-hybridization energy [12]. While U, being an intratomic quantity, might be considered the same for bulk Ce and single-atom Ce contacts, the latter may be strongly reduced via the decrease in $4f$-$(sd)^3$ hybridization. Furthermore, the effectively one-dimensional contact would entail an additional reduction of the bandwidth which, in a tight-binding model,

is proportional to the number of nearest neighbors [33]. This would lead to a strong tendency of pushing the contact towards the Mott-insulating side compared to the bulk. Thus, our observation of nearly delocalized $4f$ electrons participating in electronic conduction is at variance with the MT model for the γ-α transition in the contact region.

In the KVC model, the $4f$ electrons are nearly localized and exhibit a stable moment in both α- and γ-Ce but experience a different screening by the sd conduction electrons, resulting in unscreened moments in γ-Ce and screened moments in α-Ce. Spin fluctuations give rise to the phase transition [34,35]. The KVC is corroborated by x-ray diffraction and x-ray emission spectroscopy [36,37] and has been predicted to occur at the nanoscale down to the dimer level [38]. Experiments and first-principles calculations suggest that Ce has a low-temperature critical point at negative pressures [39,40] and is therefore close to being quantum critical [15].

One would expect that, since the $4f$-$(sd)^3$ hybridization is primarily with neighboring atoms, the Kondo temperature $T_K \approx 790$ K for α-Ce [35] would be strongly reduced. However, Kondo-like behavior might still be observed as long as T_K exceeds the measuring temperature of 4.2 K. It is important to point out that in one-dimensional metals the Kondo effect leads to an *enhancement* of the conductance, as shown in numerous examples [41–44]. We are therefore led to the conclusion that although the hybridization between conduction electrons and the $4f$ electron in the single atom of the contact very likely is reduced, the α-phase-rich q-Ce contacts facilitate f-electron transport across the junction, which is qualitatively in line with the KVC model.

V. CONCLUSION

Cerium wires with different fractions of α phase were obtained by rapid cooling or annealing. The α-phase fraction was estimated by x-ray diffraction and resistivity measurements. Single-atom contacts obtained by mechanically controlled break junctions showed an enhanced conductance compared to transition metals and to the rare-earth metals Gd and Dy. The analysis of the last-plateau conductance of various samples suggests that contacts obtained from α-phase-rich material facilitate f-electron transport across the junction and that the enhanced conductance of Ce is due to the additional contribution of the f level to the total conductance. Of course, theoretical calculations are required to further support this hybridization picture.

ACKNOWLEDGMENT

We thank K. Held, Z. Fisk, J. Schmalian, and E. Scheer for valuable discussions and W. Kittler for help with the annealing of the Ce ingot.

[1] A. W. Lawson and T.-Y. Tang, Phys. Rev. **76**, 301 (1949).
[2] D. C. Koskimaki and K. A. Gschneidner, Jr., in *Handbook on the Physics and Chemistry of Rare Earths*, edited by L. E. Karl and A. Gschneidner, Jr. (Elsevier Science, Amsterdam, The Netherlands, 1978), Vol. 1, pp. 337–377.
[3] D. C. Koskimaki and K. A. Gschneidner, Phys. Rev. B **11**, 4463 (1975).
[4] J. Wittig, Phys. Rev. Lett. **21**, 1250 (1968).
[5] I. Loa, E. I. Isaev, M. I. McMahon, D. Y. Kim, B. Johansson, A. Bosak, and M. Krisch, Phys. Rev. Lett. **108**, 045502 (2012).
[6] A. F. Schuch and J. H. Sturdivant, J. Chem. Phys. **18**, 145 (1950).
[7] D. R. Gustafson, J. D. McNutt, and L. O. Roellig, Phys. Rev. **183**, 435 (1969).
[8] U. Kornstädt, R. Lässer, and B. Lengeler, Phys. Rev. B **21**, 1898 (1980).
[9] R. Podloucky and D. Glötzel, Phys. Rev. B **27**, 3390 (1983).
[10] F. Patthey, B. Delley, W. D. Schneider, and Y. Baer, Phys. Rev. Lett. **55**, 1518 (1985).
[11] B. I. Min, H. J. F. Jansen, T. Oguchi, and A. J. Freeman, Phys. Rev. B **34**, 369 (1986).
[12] B. Johansson, Philos. Mag. **30**, 469 (1974).
[13] K. Held, A. K. McMahan, and R. T. Scalettar, Phys. Rev. Lett. **87**, 276404 (2001).
[14] L. de' Medici, A. Georges, G. Kotliar, and S. Biermann, Phys. Rev. Lett. **95**, 066402 (2005).
[15] N. Lanatá, Y.-X. Yao, C.-Z. Wang, K.-M. Ho, J. Schmalian, K. Haule, and G. Kotliar, Phys. Rev. Lett. **111**, 196801 (2013).
[16] M. K. Wilkinson, H. R. Child, C. J. McHargue, W. C. Koehler, and E. O. Wollan, Phys. Rev. **122**, 1409 (1961).
[17] E. P. Gibbons, E. M. Forgan, and K. A. McEwen, J. Phys. F **17**, L101 (1987).
[18] B. Amadon, F. Jollet, and M. Torrent, Phys. Rev. B **77**, 155104 (2008).
[19] D. Koskimaki, K. Gschneidner, and N. Panousis, J. Cryst. Growth **22**, 225 (1974).
[20] N. Agraït, A. L. Yeyati, and J. M. van Ruitenbeek, Phys. Rep. **377**, 81 (2003).
[21] E. Scheer, N. Agraït, J. C. Cuevas, A. L. Yeyati, B. Ludoph, A. Martín-Rodero, G. R. Bollinger, J. M. van Ruitenbeek, and C. Urbina, Nature (London) **394**, 154 (1998).
[22] M. Müller, R. Montbrun, M. Marz, V. Fritsch, C. Sürgers, and H. v. Löhneysen, Nano Lett. **11**, 574 (2011).
[23] B. Olivera, C. Salgado, J. L. Lado, A. Karimi, V. Henkel, E. Scheer, J. Fernández-Rossier, J. J. Palacios, and C. Untiedt, Phys. Rev. B **95**, 075409 (2017).
[24] R. Vardimon, M. Matt, P. Nielaba, J. C. Cuevas, and O. Tal, Phys. Rev. B **93**, 085439 (2016).
[25] K. Gschneidner, R. Elliott, and R. McDonald, J. Phys. Chem. Solids **23**, 555 (1962).
[26] N. R. James, S. Legvold, and F. H. Spedding, Phys. Rev. **88**, 1092 (1952).
[27] K. Ueda, J. Phys. Soc. Jpn. **43**, 1497 (1977).
[28] J. Li, W.-D. Schneider, R. Berndt, and B. Delley, Phys. Rev. Lett. **80**, 2893 (1998).
[29] M. A. Schneider, L. Vitali, P. Wahl, N. Knorr, L. Diekhöner, G. Wittich, M. Vogelgesang, and K. Kern, Appl. Phys. A **80**, 937 (2005).
[30] M. Ternes, A. J. Heinrich, and W.-D. Schneider, J. Phys.: Condens. Matter **21**, 053001 (2009).

[31] N. Néel, J. Kröger, L. Limot, K. Palotas, W. A. Hofer, and R. Berndt, Phys. Rev. Lett. **98**, 016801 (2007).
[32] E. Weschke, C. Laubschat, T. Simmons, M. Domke, O. Strebel, and G. Kaindl, Phys. Rev. B **44**, 8304 (1991).
[33] N. W. Ashcroft and N. D. Mermin, *Solid State Physics* (Saunders College, Philadelphia, PA, 1971).
[34] M. Lavagna, C. Lacroix, and M. Cyrot, Phys. Lett. A **90**, 210 (1982).
[35] J. W. Allen and R. M. Martin, Phys. Rev. Lett. **49**, 1106 (1982).
[36] M. J. Lipp, D. Jackson, H. Cynn, C. Aracne, W. J. Evans, and A. K. McMahan, Phys. Rev. Lett. **101**, 165703 (2008).
[37] M. J. Lipp, A. P. Sorini, J. Bradley, B. Maddox, K. T. Moore, H. Cynn, T. P. Devereaux, Y. Xiao, P. Chow, and W. J. Evans, Phys. Rev. Lett. **109**, 195705 (2012).
[38] M. Casadei, X. Ren, P. Rinke, A. Rubio, and M. Scheffler, Phys. Rev. Lett. **109**, 146402 (2012).
[39] J. D. Thompson, Z. Fisk, J. M. Lawrence, J. L. Smith, and R. M. Martin, Phys. Rev. Lett. **50**, 1081 (1983).
[40] J. C. Lashley, A. C. Lawson, J. C. Cooley, B. Mihaila, C. P. Opeil, L. Pham, W. L. Hults, J. L. Smith, G. M. Schmiedeshoff, F. R. Drymiotis *et al.*, Phys. Rev. Lett. **97**, 235701 (2006).
[41] M. J. Iqbal, R. Levy, E. J. Koop, J. B. Dekker, J. P. de Jong, J. H. M. van der Velde, D. Reuter, A. D. Wieck, R. Aguado, Y. Meir *et al.*, Nature (London) **501**, 79 (2013).
[42] J. Park, A. N. Pasupathy, J. I. Goldsmith, C. Chang, Y. Yaish, J. R. Petta, M. Rinkoski, J. P. Sethna, H. D. Abruña, P. L. McEuen *et al.*, Nature (London) **417**, 722 (2002).
[43] W. Liang, M. P. Shores, M. Bockrath, J. R. Long, and H. Park, Nature (London) **417**, 725 (2002).
[44] W. G. v. d. Wiel, S. D. Franceschi, T. Fujisawa, J. M. Elzerman, S. Tarucha, and L. P. Kouwenhoven, Science **289**, 2105 (2000).